Available online at www.sciencedirect.com
SCIENCE DIRECT®
ELSEVIER
Nuclear Instruments and Methods in Physics Research A 551 (2005) 364–374
NUCLEAR INSTRUMENTS & METHODS IN PHYSICS RESEARCH Section A
www.elsevier.com/locate/nima

The focal plane detector of the magnetic spectrometer PRISMA

S. Beghini[a,*], L. Corradi[b], E. Fioretto[b], A. Gadea[b], A. Latina[b], G. Montagnoli[a], F. Scarlassara[a], A.M. Stefanini[b], S. Szilner[b,1], M. Trotta[b,2], A.M. Vinodkumar[b,3]

[a]*Dipartimento di Fisica, Università di Padova and INFN Sezione di Padova, I-35131 Padova, Italy*
[b]*INFN, Laboratori Nazionali di Legnaro,I-35020 Legnaro, Padova, Italy*

Received 23 June 2005; accepted 24 June 2005
Available online 18 July 2005

Abstract

The characteristics and performance of the focal plane detector system developed for the magnetic spectrometer PRISMA are presented. It is composed of a multi-wire parallel plate avalanche counter (providing X, Y and timing signals) followed by a multi-parametric transverse field ionization chamber array (providing multiple ΔE signals). The detector array has been built to match the very large acceptance of PRISMA and provides optimal performance in the complete identification (nuclear charge, energy and mass) of nuclei produced in heavy-ion binary reactions.

PACS: 29.30.−h; 29.30.Aj; 29.40.Cs; 29.40.Gx

Keywords: Heavy-ion focal plane detector; Parallel plate avalanche counter; Timing and position-sensitive detector; Ionization chamber; Magnetic spectrometer

1. Introduction

High-resolution detection of nuclei produced in heavy-ion reactions at energies in the range ~1–10 MeV/amu often exploits magnetic spectrographs in conjunction with sophisticated focal plane detectors [1]. A large solid angle and a large ion-optical dispersion imply the need of covering a large surface at the focal plane and, from this point of view, gas detectors are very convenient since they give good time, charge and energy resolutions for heavy reaction products.

The large solid angle magnetic spectrometer PRISMA [2,3] has recently become operational at the Laboratori Nazionali di Legnaro. It has been designed primarily for studying heavy-ion

*Corresponding author. Tel.: +390 49827 7238; fax: +390 49827 7102.
E-mail address: beghini@pd.infn.it (S. Beghini).
[1]Present address: Ruder Boskovic Institute, Zagreb, Croatia.
[2]Present address: INFN Sezione di Napoli, I-80126 Napoli, Italy.
[3]Present address: Department of Chemistry, Oregon State University, Corvellis, OR 97331-4003, USA.

0168-9002/$ - see front matter © 2005 Elsevier B.V. All rights reserved.
doi:10.1016/j.nima.2005.06.058

multi-nucleon transfer reactions at energies near the Coulomb barrier [4,5]. Its very high efficiency allows to study both reaction dynamics and nuclear structure properties [6] of nuclei moderately far from stability, in particular in the neutron-rich region. The main design characteristics of PRISMA are:

- solid angle = 80 msr ($\Delta\theta = 12^\circ$ in plane, $\Delta\phi = 22^\circ$ out of plane),
- 1st order resolving power $p/\Delta p = 2000$,
- maximum $B\rho = 1.2$ Tm (mass energy product $ME/q^2 = 70$ MeV amu),
- dispersion ≈ 4 cm/% $\Delta p/p$,
- energy resolution up to 1/1000,
- nuclear charge (Z) resolution $\approx 1/60$,
- mass resolution $\approx 1/300$,
- rate capability up to 100 kHz.

This performance is accomplished by software reconstruction of the trajectories, using the time, position and energy signals from the detectors. There is no hardware correction for the (very high) optical aberration of the spectrometer, since ion tracking overcomes this problem. In heavy-ion reactions, a distribution of ion charge states q is produced in the target for each energy, mass and nuclear charge. The ambiguity in the q distribution is solved by an independent measurement of the ion energy [7].

As depicted in Fig. 1, PRISMA is composed of an entrance detector based on a two-dimensional position-sensitive Micro-Channel Plates (MCP) at 25 cm from the target [8], a quadrupole lens, a 60° dipole magnet and, finally, the Focal Plane Detectors (FPD) located at a distance of ~7 m from the target.

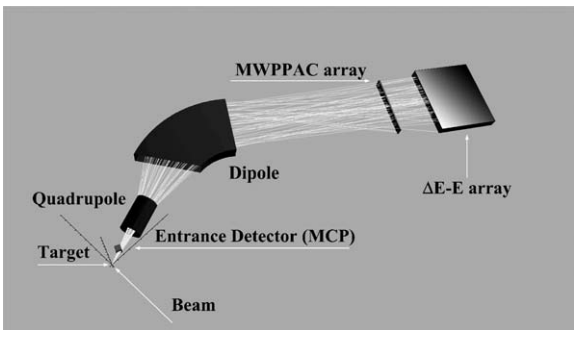

Fig. 1. Schematic view of the PRISMA spectrometer together with some ion trajectories.

The focal plane detectors must supply the following parameters:

(a) nuclear charge Z with resolution adequate to distinguish ions with Z up to ~60 and at energies 2–10 MeV/amu,
(b) total energy E with resolution ~1% for the ions of interest, in order to distinguish, together with Time-of-Flight (TOF) and position along the dispersion plane, the ion charge states selected by the spectrometer,
(c) timing signals, for TOF determination, with resolutions ~300–400 ps, which allows, together with X position (i.e. $B\rho$ of the ion), the determination of nuclear masses,
(d) two-dimensional position resolutions around 1 and 2 mm for X and Y positions, respectively.

The detector system must also have a very large area to fully exploit the acceptance and dispersion of PRISMA, thus allowing the detection of ions produced with very low cross-sections in weakly populated transfer channels. It must work in a large dynamical energy range (ions may reach the focal plane with large energy differences) maintaining the resolutions listed above for total rates up to ~100 kHz. Finally, the detector geometry has to be chosen to minimize dead spaces. The adopted solution is based on modular gas detectors, essentially an array of Parallel Plates Avalanche Counters of Multi-Wire type (MWPPAC) and multi-anode Ionization Chambers (IC).

The FPD are discussed in Section 2, while Sections 3 and 4 are dedicated to the electronic front-end layout and vacuum control system, respectively. In Section 5, performance and results will be discussed. Section 6 summarizes the main aspects of this work.

2. Focal plane detectors

2.1. MWPPAC

The X and Y positions of the reaction products at the focal plane of PRISMA are provided by a

large-area MWPPAC. A timing signal is also extracted from it in order to perform TOF measurements in coincidence with the MCP entrance detector. The MWPPAC can work with high event rate preserving a good linearity in the position determination and allowing also the rejection (within certain limits) of unwanted particles by changing the electrode voltages and gas pressure. An exploded view of the detector is shown in Fig. 2.

The detector has a three-electrode structure: a central cathode and two wire planes (X and Y anodes) orthogonally oriented with respect to each other. To prevent the deformation of the electrodes under the stress due to the large number of wires across a large surface ($13 \times 100\,cm^2$), the system is sandwiched inside two machined aluminum frames on which the printed-circuit layers (G-10) are fixed. All electrodes (with Y and the cathode assembled together) are mounted on G-10 frames and independently fixed on aluminum supports, which form the two halves of the final package. The complete MWPPAC (electrodes and metallic frames) is inserted in its own stainless-steel vessel closed on both sides by two large mylar windows ($100 \times 13\,cm^2$) facing the anodes wire planes at a distance of 3 mm. The windows are

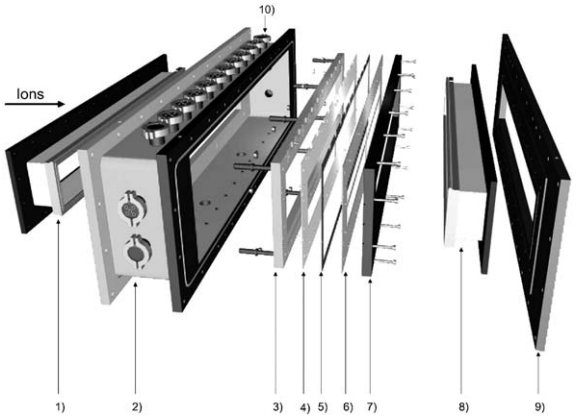

Fig. 2. Exploded view of the MWPPAC. 1) Input window, 2) vacuum vessel, 3) aluminum X frame, 4) X printed-circuit board, 5) vetronite spacer, 6) cathode-Y printed-circuit board, 7) aluminum cathode-Y frame, 8) exit window, 9) matching connection flange, 10) individual electrical connections for each section.

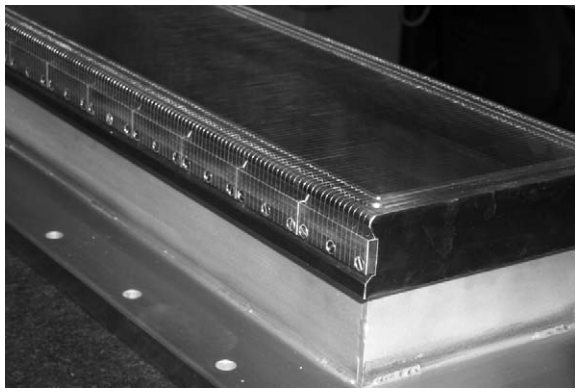

Fig. 3. Picture of part of the window support (see text).

made of 1.5 μm thick mylar foils glued on proper metallic frames and supported by 100 μm stainless-steel wires (with a step of 3.5 mm and a stress of 200 g). Fig. 3 shows a part of the window support structure.

The cathode is made of 3300 gold-plated tungsten wires, 20 μm in diameter and a spacing of 0.3 mm. The wires are fastened at both ends by soldering to a printed circuit on a 2.4 mm thick G-10 frame, which was previously fixed in its own aluminum frame.

The electrode is divided into ten equal and independent sections. Each of them has an active area of $10 \times 13\,cm^2$ and provides a timing signal for both TOF measurements and data acquisition trigger.

The X-plane is equally segmented as the cathode and each section consists of 100 gold-plated tungsten wires with 20 μm diameter and a spacing of 1 mm. The wires are soldered to a printed circuit on a 1.6 mm thick G-10 frame. The Y-plane is common to all cathode sections with 130 wires (100 cm long, with the same diameter and step as for X wires) soldered on the other side of the cathode frame. The Y wires are shorted two by two on the delay-line side producing 65 steps with 2 mm resolution. Both X and Y wires (perpendicular to each other) are symmetrically placed with respect to the cathode at a distance of 2.4 mm from it. The cathode is biased at a negative potential in the range 500–600 V at working pressures of about 7–8 mbar of isobutane gas (C_4H_{10}). The anodes are kept at ground potential through 100 kΩ resistors

at both ends. In this configuration (see [9] and references therein), the electrostatic forces on the cathode are balanced. This design avoids bending of the cathode wires which would introduce dishomogeneities in the electric field and worsen the detector performance. The position information is extracted from the anodes by using a delay-line readout. Resistor chain is avoided since the signal attenuation becomes too strong when using a large number of wires. The wires are electrically connected by discrete LC elements, mounted on the G-10 frame, with a fixed delay of 1.7 ns per wire and a characteristic impedance of 50 Ω. The total delay between the ends of each X section amounts to 170 ns. In order to minimize the dead spaces and get a better linearity, standard integrated delay lines have been avoided. Small capacitors (C) were surface mounted on the frame together with small commercial inductors (L) made of Cu wire wound on a proper ceramic support. The total delay for the Y wires is 110.5 ns. Fig. 4 shows the electrical scheme of the electrodes together with the photographs of part of the delay lines and of the wires soldered on the X and Y frames. With this choice, the dead space between adjacent sections is minimized.

In this configuration, each wire acts as an independent cell. The avalanche produced by the impinging particle is well localized in space; due to the narrow spacing between the detector planes the charge is induced mainly on a single wire and therefore the X and Y resolutions are determined by their steps (1 and 2 mm, respectively). Fig. 5 shows a picture of the MWPPAC inserted into its stainless-steel vessel.

2.2. Ionization chamber

The MWPPAC is followed (60 cm downstream) by an array of multi-parametric, multi-section transverse-field $\Delta E - E$ IC [10–12]. In order to match the large acceptance of PRISMA, the

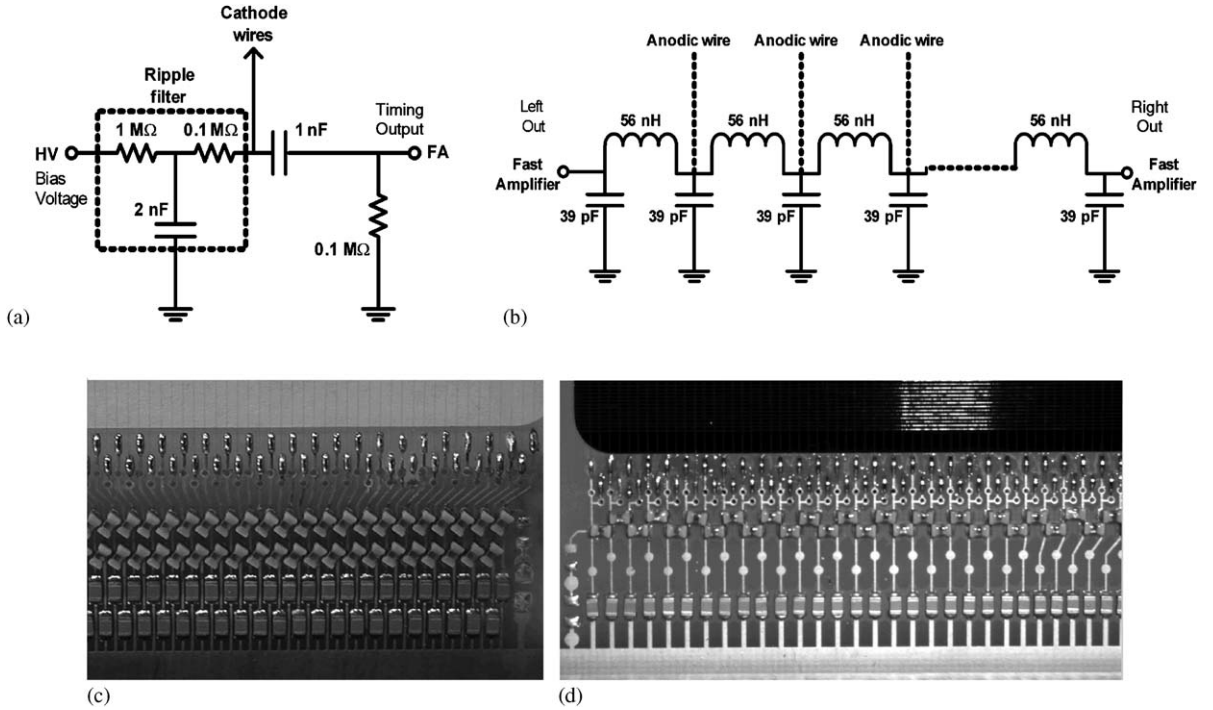

Fig. 4. (a) Electrical scheme for an individual section of the MWPPAC, (b) delay-line scheme, (c) and (d) photographs showing the details of the X and Y delay lines, respectively.

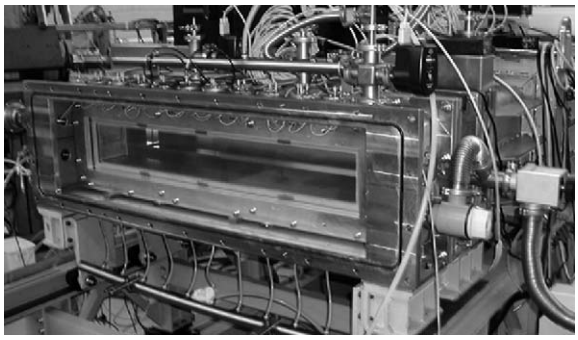

Fig. 5. Picture of the MWPPAC inserted in its vacuum vessel.

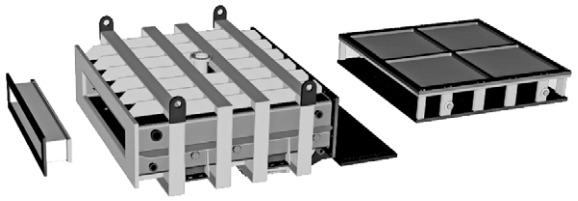

Fig. 6. Schematic view of the IC: electrode package (right), the stainless-steel vacuum vessel (center) and the entrance window (left). The electrode package can be inserted into the vessel by means of two rails with precise mechanical regulation.

dimensions are $110(X) \times 20(Y)\,\mathrm{cm}^2$ while the active depth is 120 cm. The motivations for this long depth are: (1) to be able to stop all ions produced in a nuclear reaction and entering into PRISMA, which typically have a large kinematical spread, (2) to have an ionization range long enough for heavy ions having lower kinetic energy, since in this case electric field dishomogeneities close to the huge entrance window may strongly limit the nuclear charge and energy resolutions and (3) to use low working pressures, thus minimizing the stress on the entrance window. Fig. 6 shows an exploded view of the detector assembly.

Special care has been devoted to the production of the entrance mylar window, since it has to hold a pressure as high as 100 mbar with a maximum deformation of 3 mm. The 1.5 μm thick mylar foil is glued onto a stainless-steel nose and is supported by 1000 stainless-steel wires (100 μm diameter, 1 mm step).

The wires are stretched on the metallic frame with a stress of 700 g. The basic structure is similar to the one shown in Fig. 3.

The cathode and anode electrodes of the IC are composed of 40 pads (10 sections × 4 pads) plus 28 side pads (50 mm wide) acting as guard rings for field linearization. Each pad (265 mm long, 99 mm wide) acts as an independent ΔE section. This choice is an optimum compromise between preserving good Z and E resolution over the whole focal plane (where the event rate may reach several kHz per section) and keeping the number of pads, and consequently the electronic requirements, at a reasonable level. The cathode and anode are obtained by a photoengraving process of Cu layer deposited onto a 2 mm thick G-10 plate. In order to produce the two electrodes with standard commercially available machinery, each one has been obtained by assembling four smaller pieces. In order to avoid mechanical deformation of the structure, the electrodes have been glued on suitable 25 mm thick vetronite frames.

All electrical connections are made in such a way as to minimize the cable length. The Frisch grid (common to all sections) is made of 1200 gold-plated tungsten wires with a 100 μm diameter, spaced 1 mm and 110 cm long. The wires are soldered on both sides of a G-10 frame after proper stretching (100 g). The anode-Frisch grid and cathode-Frisch grid distances are 25 and 175 mm, respectively. Fig. 7 shows a picture of the inner part of the IC.

The detector is routinely operated with methane (CH_4, 99.99% purity), which has a high electron drift velocity, thus allowing to preserve good energy resolution even with the high counting rates needed in the experiments with PRISMA. Heavy-ions heavier than $\approx {}^{40}$Ca at energies up to 6 MeV/amu are completely stopped in the active volume of the IC at a maximum pressure of 100 mbar.

The cathode pads (which are connected together) are held at ground potential while the Frisch grid is biased at a potential corresponding to a reduced electric field (E/p) in the active region of about $0.6\,\mathrm{V/(cm \times mbar)}$. The anode–cathode voltage is twice the voltage of cathode-Frisch grid. With this polarization, the shielding inefficiency of the Frisch grid is minimized. The metallic frame of the entrance window is grounded, so that the loss

Fig. 7. Inner view of the IC. The pads of anode (top) and cathode (bottom) are visible, as well as the wires of the Frisch grid in between.

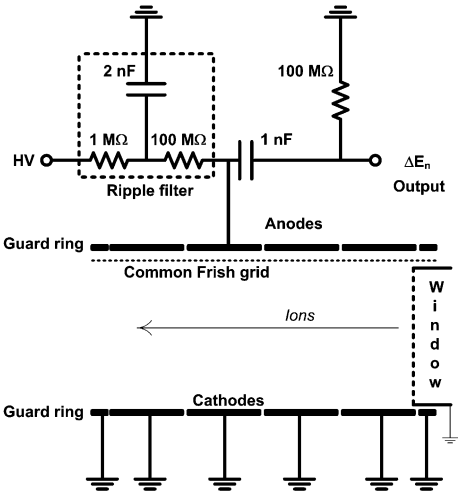

Fig. 8. Electrical scheme for one representative pad of one IC section.

of resolution due to field distortion is kept at minimum. Fig. 8 shows the electrical scheme of the IC.

3. Front-end electronics

Commercial and homemade electronics are used for processing the FPD signals. Fig. 9 presents a scheme of the electronic layout.

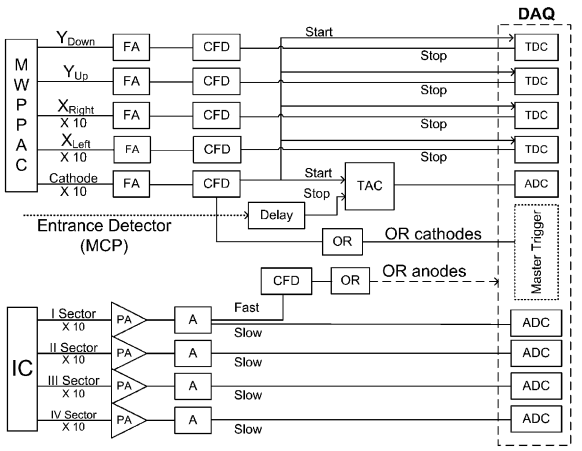

Fig. 9. Scheme of FPD front-end electronics.

The MWPPAC signals (20 for X, 2 for Y and 10 for timing) are sent to low-cost, homemade 8-channel modules fast voltage amplifiers[4] (FA). The voltage gain is 200 with differentiating and integrating constants of 10 ns. A commercial bias voltage power supply with low ripple (especially for high frequencies) and good long-term stability has been used. The FA outputs are sent to constant fraction discriminators, SEN CF 8000 for the X, Y signals and Ortec Quad 935 for the cathode ones, these last signals requiring sub-nanosecond timing resolution. The TOF is measured between the MCP entrance detector and the cathodes. X and Y positions are produced by measuring, through a common start time to digital converter (TDC), the time interval between MWPPAC timing signals (common start) and the delay-line outputs (individual stop). The OR of the cathode signals is used as master trigger for the data acquisition system (see below). Hybrid charge preamplifiers[5] with a sensitivity of 28 mV/MeV (Si equivalent) are used for the IC anodes. Their main features are a low-cost, low-noise and low-power dissipation. The hybrids have been mounted in a plug-n-play configuration on a common board

[4]Developed by the Electronic Workshop of the INFN Sezione di Padova.

[5]Developed by the Electronic Workshop of the INFN Sezione di Napoli.

that can house up to eight preamplifier modules and provides the required bias voltages. The boards (including the eight preamplifiers) are installed in aluminum boxes and placed very close to the IC anode signal outputs. The output signals of the charge preamplifiers are sent to 16-channel NIM Amplifiers (SILENA 761F) providing slow linear and fast timing outputs. Their parameters (fine and coarse gain, shaping time, pole-zero and offset) can be set by means of a RS-485 serial line connected to a PC. The amplifier gains for the different anodes of the IC have been calibrated by injecting a known charge on the corresponding preamplifier. The fast timing outputs of the amplifiers, associated to the first pad of each section of the IC, are sent to 8-channel SEN CF 8000 constant fraction discriminators that allow to set a threshold and extract suitable signals that can be used as independent triggers.

The FPD provides a total of 72 signals (40 ΔE anodes, 10 cathodes, 20 X and 2 Y positions) with a maximum trigger rate up to 100 kHz (typically 10–20 kHz). All signals are processed by the PRISMA data acquisition system based on VME standard protocol whose front-end is composed of 32-channel ADCs, 32-channel TDCs and a 32-channel scaler. The computing services (Histogram Server, Tape/Disk Server) are based on the Linux OS, and run on dual processor PC.

4. The FPD vacuum system

Fig. 10 shows schematically the five vacuum regions in which the FPD is divided (from right to the left: preMWPPAC, MWPPAC, post-MWPPAC, preIC and IC). Two big gate valves (V-13, V-12) and three 1.5 μm thick mylar windows separate the different sections. The two gate valves separate the detector volumes and allow to perform the vacuum and venting operations independently for the IC, the MWPPAC and the rest of the spectrometer.

The choice of using the MWPPAC section as a second barrier for the unavoidable gas leak coming from the IC window (because of the large size and relatively high pressure) allows to have a very good vacuum in the spectrometer region

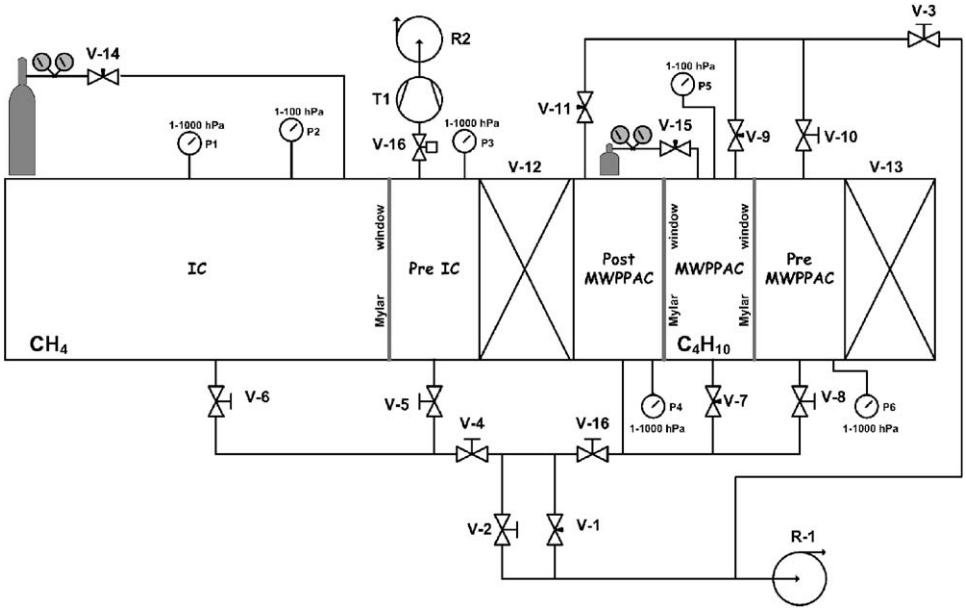

Fig. 10. Vacuum layout of the FPD. Ions analyzed by PRISMA enter the detector system from the right of the picture.

where a pressure of at least $2–3 \times 10^{-6}$ mbar must be maintained for good MCP detector performance. The gas flowing systems for both detectors (not indicated in Fig. 10) have been assembled and properly tested. However, in experiments where the event rates are kept at few kHz, no deterioration of the detector performance has been evidenced without gas flow, on a time range of one day.

5. In-beam tests and performances

In-beam tests have been done using various heavy-ion reactions. Ions with $A \approx 30–100$ amu at specific energies of 2–5 MeV/amu have been analyzed by the spectrometer. Performances very close to the design goals have been demonstrated. The same characteristics have been confirmed during the first experimental campaign of PRISMA.

Fig. 11 left panels show X (up) and Y (bottom) position spectra of the MWPPAC obtained detecting the Ca-like particles produced in the transfer reaction of 152 MeV ^{40}Ca + ^{96}Zr. The obtained experimental position resolutions of 1 mm (X) and 2 mm (Y) are in agreement with the design characteristics of the detector. Good peak-to-valley ratios of the spectra are obtained. The peak (and the hole) in the central zone corresponds to two wires shorted to get the absolute geometrical reference used for the position calibration. The different shapes of the X and Y spectra are due to the PRISMA focusing properties, i.e. dispersing in X and focusing in Y. The detector has an efficiency very close to 100% for a wide range of heavy ions ($A \sim 40-200$ amu) and energies, when compared with a reference number of events collected in the IC operated in the self-trigger mode. As counter check, in the normal trigger operation (with MWPPAC cathodes as master trigger), selecting the true events in the matrix X-TOF, an IC efficiency of ~85% has been found in agreement with the geometrical transparency of the wire grids between the cathodes of the MWPPAC and the active volume of the IC.

In the same figure (right panels), the overall measured time resolution (up) is shown. The measured TOF spectrum is constructed choosing a narrow gate 1×20 mm^2 ($\Delta\theta = 0.23^\circ$, $\Delta\phi = 4.6^\circ$) in the MCP detector and 1×13 mm^2 (one X wire of the central section) in the MWPPAC. In addition, a small gate is set on the quasi-elastic energy peak of the IC in order to select a narrow range of trajectories. With these conditions, a FWHM resolution of 630 ps is measured. The TOF width is due to the intrinsic time resolution of the start and stop detectors, the contribution due to the energy straggling in the ^{96}Zr target (a vertical strip 1 mm wide, 200 μg/cm^2 thick, evaporated onto a 20 μg/cm^2 carbon backing) and the beam spot size. These contributions have been calculated with a spot size of 1 mm^2 and with the same geometrical conditions as the measured TOF. The result is reported in Fig. 11 (right panel, bottom). Taking into account that, through an independent measurement, the FWHM MCP detector resolution was deduced to be ≈ 300 ps [8], an intrinsic time resolution of 300 ps has been derived for the MWPPAC.

In Fig. 12, $\Delta E - E$ matrices and mass spectra produced in the reaction ^{82}Se + ^{238}U are reported. A beam of ^{82}Se has been accelerated at 505 MeV onto a ^{238}U strip target (1 mm wide, 400 μg/cm^2 thick on 20 μg/cm^2 carbon backing). The Se-like reaction products were analyzed by the spectrometer placed at the grazing angle ($\theta_{LAB} = 64^\circ$). In Fig. 12(a), a full ΔE–E matrix is displayed (10 sections of the IC summed all together). Z and E resolutions $Z/\Delta Z \approx 60$ and $\Delta E/E \approx 1.5\%$ have been obtained. The large dynamical acceptance of the IC has to be noticed. In fact, events deriving from deep inelastic collisions and fission are visible (top of the figure) together with the quasi-elastic ones even if the IC and spectrometer conditions were set for the quasi-elastic reaction products.

The figure shows the $\Delta E - E$ matrix for two different sections at the right (panel c) and left (panel d) border of the FPD. It can be seen that even in these cases good resolutions are preserved. The spot-like structures, more visible in the section

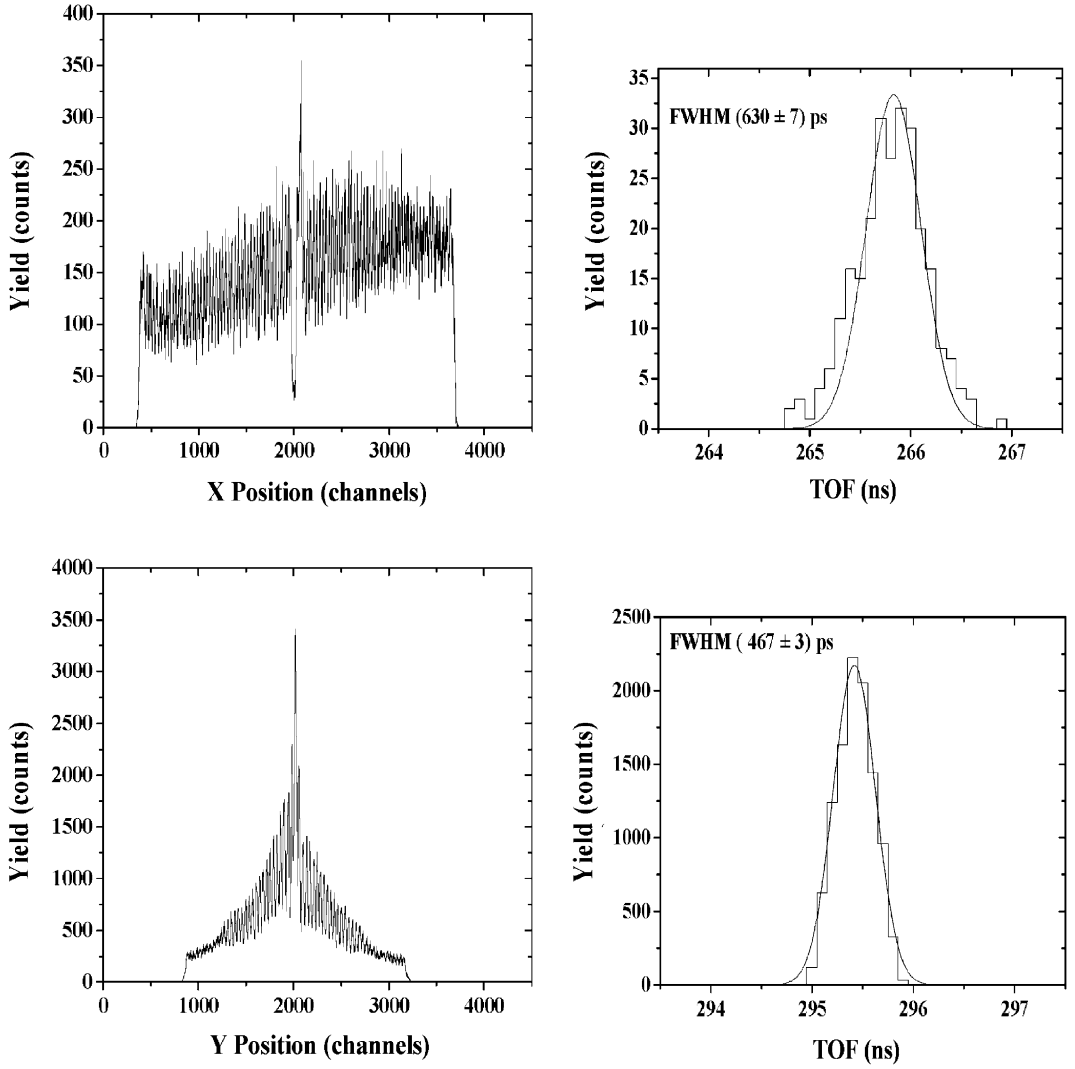

Fig. 11. Left panels: measured X and Y position spectra for the reaction 152 MeV ^{40}Ca + ^{96}Zr, where the central angle of PRISMA was $\theta = 75^{\circ}$. Right panels: measured (up) and calculated (bottom) time resolutions for the same reaction (see text). The absolute time calibration of the two TOF spectra are different. Only a part of the full statistics is shown. Gaussian fits of the spectra are shown as lines.

of panel (c), are due to the magnetic rigidity (momentum over charge state) selection of the spectrometer.

Panel (b) shows the mass spectrum of the Ge isotopes obtained after ion-track reconstruction [13]. A mass resolution $\Delta A/A \sim 1/270$ is obtained confirming the very good performance of the FPD and MCP detectors.

6. Summary

The most relevant feature of the PRISMA FPD system is its ability to measure time, positions, energy loss and total energy of the analyzed ions over a large area and with good resolution. A very high reliability has been demonstrated during several in-beam test runs and measurements

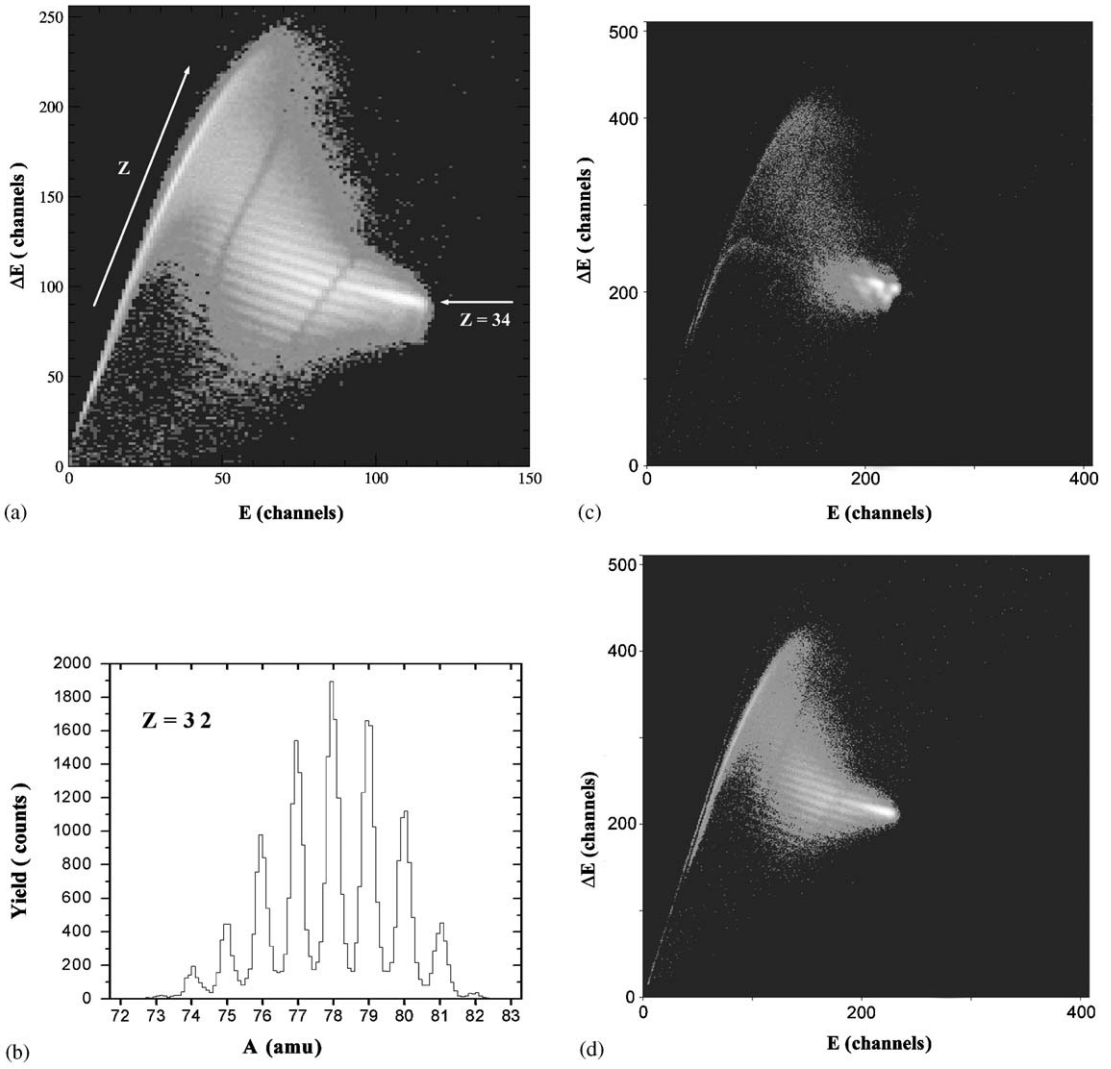

Fig. 12. $\Delta E - E$ matrices and a mass spectrum produced in the reaction 505 MeV ^{82}Se + ^{238}U (see text). Only part of the total statistics is shown. The diagonal lines in the $\Delta E - E$ matrix are due to the thresholds of the ADC.

(^{32}S, ^{40}Ca, ^{56}Fe, ^{64}Ni, ^{82}Se, ^{90}Zr beams scattered by heavy targets), and ions with $A \geqslant 30-40$ are detected with about 100% efficiency. Performance very close to the design goals for both MWPPAC and IC are routinely achieved. In particular, a mass and nuclear charge resolutions of $\sim$1/270 and $\sim$1/60 are obtained by TOF, X–Y and $\Delta E - E$ measurements. The possibility of selecting the $\Delta E - E$ combination by adding, off-line, the IC sections in a suitable way, allows to optimize the identification of different kind of fragments over the whole focal plane.

Acknowledgments

The authors wish to thank Mr. L. Barcellan, M. Cavicchi, S. Marchini, V. Schiavon, P. Zatti for

the construction of the MWPPAC electrodes and the detectors assembling, and for providing the fast amplifiers. We are thankful to Mr. F. Veronese for his constant technical assistance in the designing and mounting of all mechanical parts of the detectors. We also acknowledge the precious collaboration of Mr. L. Doná.

Grateful thanks are due to INFN Section of Napoli, in particular to Mr. M. Di Pietro and Dr. M. Romoli for the design and test of the preamplifiers for the IC.

References

[1] H. Enge, Nucl. Instr. and Meth. A 162 (1979) 161.
[2] A. Stefanini, et al., L.N.L.- I.N.F.N. (REP) 120/97.
[3] A. Stefanini, et al., Nucl. Phys. A 701 (2002) 217c;
F. Scarlassara, et al., Nucl. Phys. A 746 (2004) 195c;
A. Latina, et al., Nucl. Phys. A 734 (2004) E1.
[4] L. Corradi, et al., Phys. Rev. C 66 (2002) 024606.
[5] S. Szilner, et al., Phys. Rev. C 71 (2005) 044610.
[6] A. Gadea, et al., Eur. Phys. J. A 20 (2004) 193.
[7] D. Schüll, in: W. Von Oertzen (Ed.), Lecture Notes in Physics, vol. 178, Proceedings of the Symposium on "Detectors in Heavy-Ion Reactions", HMI Berlin, 6–8 October 1982, Springer, Berlin, Heidelberg, 1983, p. 80.
[8] G. Montagnoli, et al., Nucl. Instr. and Meth. A (2005) in press.
[9] S. Beghini, et al., Nucl. Instr. and Meth. A 362 (1995) 526.
[10] K. Rudolph, et al., Nucl. Instr. and Meth. A 204 (1983) 407.
[11] K. Kusterer, et al., Nucl. Instr. and Meth. A 177 (1980) 485.
[12] U. Quade, Ph.D. Thesis, Universität München, 1983.
[13] A. Latina, et al., LNL Annual Report 2004
A. Latina, et al., Ph.D. Thesis, Università di Torino, 2005.